JPE 17-2-16

https://doi.org/10.6113/JPE.2017.17.2.476
ISSN(Print): 1598-2092 / ISSN(Online): 2093-4718

Combining Model-based and Heuristic Techniques for Fast Tracking the Global Maximum Power Point of a Photovoltaic String

Ji-Ying Shi*, Fei Xue†, Le-Tao Ling*, Xiao-Fei Li**, Zi-Jian Qin*, Ya-Jing Li*, and Ting Yang*

*School of Electrical and Automation Engineering, Tianjin University, Tianjin, China
†Electric Power Research Institute, State Grid Ningxia Electric Power Company (NEPC), Yinchuan, China
**State Grid Electric Power Research Institute, Nanjing, China

Abstract

Under partial shading conditions (PSCs), multiple maximums may be exhibited on the *P-U* curve of string inverter photovoltaic (PV) systems. Under such conditions, heuristic methods are invalid for extracting a global maximum power point (GMPP); intelligent algorithms are time-consuming; and model-based methods are complex and costly. To overcome these shortcomings, a novel hybrid MPPT (MPF-IP&O) based on a model-based peak forecasting (MPF) method and an improved perturbation and observation (IP&O) method is proposed. The MPF considers the influence of temperature and does not require solar radiation measurements. In addition, it can forecast all of the peak values of the PV string without complex computation under PSCs, and it can determine the candidate GMPP after a comparison. Hence, the MPF narrows the searching range tremendously and accelerates the convergence to the GMPP. Additionally, the IP&O with a successive approximation strategy searches for the real GMPP in the neighborhood of the candidate one, which can significantly enhance the tracking efficiency. Finally, simulation and experiment results show that the proposed method has a higher tracking speed and accuracy than the perturbation and observation (P&O) and particle swarm optimization (PSO) methods under PSCs.

Key words: Model-based, MPPT, Multiple local maximum, Partial shading, PV system

I. INTRODUCTION

Photovoltaic energy is one of most important renewable energy sources. Low carbon, no noise, no pollution and other advantages have made it a popular choice in the world today. The worldwide growth of photovoltaic energy has been fitting an exponential curve for more than two decades. To provide sufficient electricity to the load, multiple PV modules need to be connected in series or parallel to form a PV string or array. A PV string would be preferred as a configuration, because it has the least power losses under partial shading conditions (PSCs). Maximum power point tracking (MPPT) is an indispensable technique for maximizing power output and reducing energy losses. Many experts and scholars have made a number of studies in this field, and put forward many methods and strategies. These methods can be broadly divided into three main categories of heuristic methods, intelligent methods and model-based techniques.

Several heuristic MPPT methods have been proposed in the literature. Representative methods are the perturbation and observation (P&O) method [1]-[4], incremental conductance (INC) algorithm [5]-[7], fuzzy logic control search method [8], and hill climbing (HC) method [9]-[10]. Additionally, Ref. [11] and [12] proposed an effective beta method for tracking the MPP under normal irradiance conditions and solve the conflict between steady-state oscillations and dynamic speed. These heuristic methods perform extremely well under normal irradiance conditions. However, PV modules are generally installed in outdoor environments, and they are prone to electrical faults as a

Manuscript received Mar. 17, 2016; accepted Dec. 3, 2016
Recommended for publication by Associate Editor Yihua Hu .
†Corresponding Author: tjuxf1010@126.com
Tel: +86-022-2740-6071, State Grid Ningxia Electric Power Company
*School of Electrical and Automation Eng., Tianjin University, China
**State Grid Electric Power Research Institute, China

result of PSCs and hotspots [13]-[14]. It is common to experience PSCs due to dust, clouds or shadows. Under PSCs, the *P-U* curves of a PV array present multiple peaks. As a result, heuristic methods can become invalid and fall into a local maximum power point (LMPP) [15], which leads to energy losses for the PV systems. Ref. [16] showed that PV systems power losses can be as high as 70% under PSCs.

To heighten the efficiency of PV systems under PSCs, researchers have proposed a variety of intelligent algorithms to extract the GMPP in recent years, including particle swarm optimization (PSO) [17]-[18], ant colony optimization (ACO) [19], firefly algorithm (FA) [20]-[21], cuckoo search (CS) [22]-[23], artificial bee colony (ABC) [24], etc. These intelligent algorithms are capable of tracking the GMPP. However, they spend a great deal of time on the search, and the existence of random variables makes the search time stochastic.

In addition, model-based MPPT methods have been put forward due to the rapid development of mathematical model theories in recent years. These model theories offer a new direction for development of MPPT methods. However, they still have several defects. The method proposed in [25], is highly CPU-intensive and requires solar radiation sensors that are quite expensive (around the cost of six 120W solar modules). The methods in [26] and [27] require more expensive high-accuracy sensors for temperature and irradiance measurements, and operate only under normal irradiance conditions. The method in [28] requires voltage and current sensors in every PV module, which significantly increases expenditures. On the other hand, it results in an enormous amount of data transfer to the PV system and is ineffective under PSCs. The method in [29] eliminates temperature sensor by relying on a set of equations capable of estimating the PV module temperature through utilizing the current and voltage sensor under normal irradiance conditions. However, it is also ineffective under PSCs. Although the method proposed in [30] can solve the partial shading problem, it requires solar radiation sensors. Additionally, it need to make calculations with a modified Newton iteration, which leads to huge calculations and low efficiency. As a result, it would undoubtedly require a high-performance DSP to support such huge calculations. The authors of [31] proposed a thermography-based MPPT scheme to address PV partial shading faults. It shows a novel idea for the MPPT idea but the thermography camera is costly.

To overcome the above shortcomings, this paper proposes a novel method combining the MPF and the IP&O to track the GMPP of a PV string under PSCs. The variation of the peak value of the PV string under uniform/non-uniform irradiation was analyzed in this study. In addition, a model-based peak forecasting method (MPF) is established according to the analyze results. First, the MPF forecasts each of the peak values of the PV string and locates the candidate one. Then the IP&O searches for the real GMPP in the neighborhood of the candidate one.

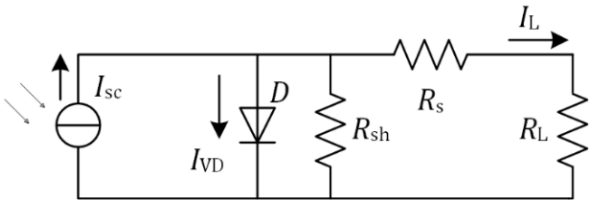

Fig. 1. Single diode model of PV cell.

This method has the following advantages when compared to the former two. (1) The proposed algorithm applies MPF to effectively decrease the blindness of the global search under unknown environments and saves a lot of search time while intelligent algorithms cost a lot of time. (2) During the initialization of the proposed algorithm, the system calculates the relevant parameters according to the voltage, current and temperature of the operating point which includes environmental factors. Hence, additional irradiance sensors are unnecessary. This makes the system more reliable, easier to maintain and cost-effective. (3) Compared with the method in [30], the proposed algorithm is simple enough to realize in practical engineering applications. It does not use a Lambert functions and does not need the Newton method. Consequently it has fewer calculations, a higher velocity, a higher accuracy and a lower performance requirements for the DSP.

In this paper, a mathematical model of the photovoltaic cells and calculation methods for some of the parameters are presented in Section 2. Section 3 introduces the principle of short circuit current measurement used in this paper, and draws the conclusion of the MPF under PSCs based on Section 2. Section 4 presents some simulation and experimental results. Finally, the paper is summarized in Section 5.

II. THEORETICAL MODEL OF A PV CELL

A PV cell can be modeled by a current source I_{sc}, a diode D, and resistances R_s and R_{sh} as shown in Fig. 1. R_L is the load resistance, and I_{sc} is the short circuit current which is closely related to irradiation and temperature [32]-[34].

The diode current I_{VD} and saturation current I_{D0} [35] are expressed in the following:

$$I_{VD} = I_{D0}\left(e^{\frac{qI_L R_s}{n_i kT}} - 1\right) \tag{1}$$

$$I_{D0} = AqN_C N_V \left[\frac{1}{N_A}\left(\frac{D_n}{\tau_n}\right)^{\frac{1}{2}} + \frac{1}{N_D}\left(\frac{D_p}{\tau_p}\right)^{\frac{1}{2}}\right] e^{-\frac{E_g}{kT}} \tag{2}$$

The ideality factor parameter [36-37] is defined as:

$$a \equiv \frac{n_1 kT}{q} \tag{3}$$

a_{ref} and I_{D0}, under standard reference conditions, can be calculated as follows:

$$a_{ref} = \frac{2U_{m,ref} - U_{oc,ref}}{\frac{I_{sc,ref}}{I_{sc,ref} - I_{m,ref}} + \ln\left(1 - \frac{I_{m,ref}}{I_{sc,ref}}\right)} \tag{4}$$

$$I_{D0,ref} = I_{sc,ref} \cdot e^{-\frac{U_{oc,ref}}{a_{ref}}} \tag{5}$$

For the same PV cell materials, the parameter a, the saturation current I_{D0} and the energy bandgap E_g are only affected by the cell temperature T. Therefore, it is easy to calculate a, I_{D0} and E_g according to the temperature of the PV cell:

$$a = \frac{Ta_{ref}}{T_{ref}} \tag{6}$$

$$I_{D0} = I_{D0,ref}\left(\frac{T}{T_{ref}}\right)^3 e^{\frac{1}{k}\left(\frac{E_g}{T}\Big|_{T_{ref}} - \frac{E_g}{T}\Big|_{T_c}\right)} \tag{7}$$

$$\frac{E_g}{E_{g,T_{ref}}} = 1 - 0.0002677\left(T - T_{ref}\right) \tag{8}$$

The relationship between the load voltage U_L and the load current I_L can be expressed as follows:

$$I_L = I_{sc} - I_{D0}\left[e^{\frac{q(U_L - I_L R_s)}{n_1 kT}} - 1\right] - \frac{U_L + I_L R_s}{R_{sh}} \tag{9}$$

In general, the photovoltaic cell series resistor R_s is small and the parallel resistor R_{sh} is very large. During an ideal calculation, Equation (9) can be rewritten as follows:

$$U_L = a\ln\left(\frac{I_{sc} - I_L}{I_{D0}} + 1\right) \tag{10}$$

I_{D0} is an extremely small value. Therefore, Equation (10) can be rewritten as:

$$U_L \approx a\ln\left(\frac{I_{sc} - I_L}{I_{D0}}\right) \tag{11}$$

In addition, U_{oc} and I_{sc} can be calculated as:

$$U_{oc} = a\ln\left(\frac{I_{sc}}{I_{D0}} + 1\right) \approx a\ln\left(\frac{I_{sc}}{I_{D0}}\right) \tag{12}$$

The cell temperature T can be obtained by a temperature sensor, and the parameters a and I_{D0} can be achieved from Equation (6) and (7). Consequently, after the initialization of the algorithm, the influence of the cell temperature T is taken into account by the values of a and I_{D0}.

III. Model-based Peak Forecasting Method

A. Method of Measuring the Short Circuit Current

A novel short current method for a PV string is proposed.

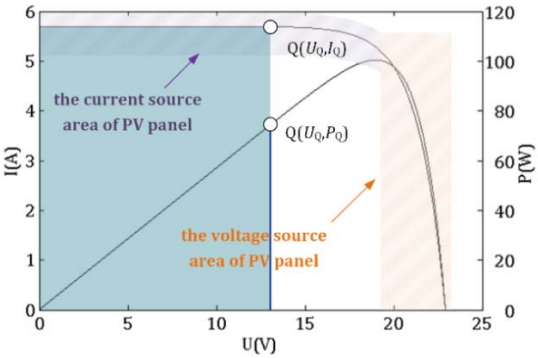

Fig. 2. *I-U* curve and *P-U* curve of the PV module.

This method eliminates short circuits and a huge number of current sensors.

An *I-U* curve of a PV module is shown in Fig. 2. The change of the current is insignificant in the purple shaded area, the PV cell can be approximated as an ideal current source, and it can be called the current source region. Therefore, the orange shaded area can be called the current source region. The PV module works at the operating point Q (U_Q, I_Q). The blue area is the output power of the PV module P_Q. When the module works in the current source area, it can be considered that the current does not change, and that the short circuit current I_{sc} can be replaced by the operating point current I_Q:

$$I_{sc} \approx I_Q \tag{13}$$

The slope of the *P-U* curve can be approximated as a substitute for the short circuit current.

B. Peak Forecasting Method for a Single Module

When a single PV module is operating under the uniform irradiation condition (UIC), there is single peak in the *P-U* curve. As shown in Equation (14) and (15), the voltage factor k_1 is the ratio of U_m to U_{oc}, and the current factor k_2 is the ratio of I_m and I_{sc}.

$$k_1 = \frac{U_m}{U_{oc}} \tag{14}$$

$$k_2 = \frac{I_m}{I_{sc}} \tag{15}$$

k_1 and k_2 are very important parameters in MPPT. To obtain the relationship between environmental factors (temperature T and irradiation S) and these parameters, two groups of simulation experiment have been designed. The environment temperature T was set as 25℃, and the irradiation was changed S from 1000W/m^2 to 100W/m^2. Similarly, the environment irradiation was set as 1000W/m^2, and the temperature T was changed from 40℃ to -10℃. From Fig. 3, it is easy to see that k_1 and k_2 have an extremely small variation amplitude. Therefore, in practical applications, it can be considered that the values of k_1 and k_2 are constant, and are not affected by environment changes [38].

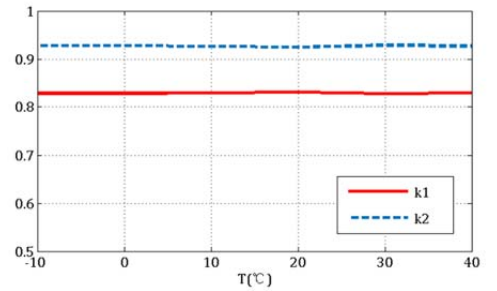

(a)

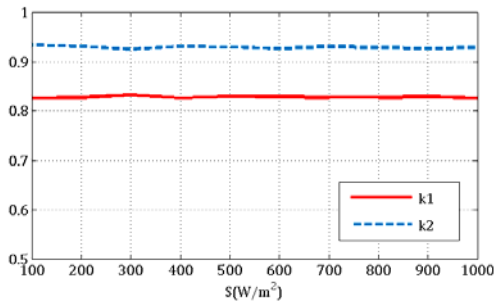

(b)

Fig. 3. Change trend of k_1 and k_2. (a) a broad temperature range (S=1000W/m^2), (b) a broad irradiation range (T=25℃).

According to Equations (12), (14) and (15), U_m and I_m can be expressed as Equation (16) and (17):

$$U_m = k_1 a \ln\left(\frac{I_{sc}}{I_{D0}}\right) \tag{16}$$

$$I_m = k_2 I_{sc} \tag{17}$$

The maximum power value P_m can be calculated according Equation (18):

$$P_m = U_m I_m = k_1 a \ln\left(\frac{I_Q}{I_{D0}}\right) k_2 I_Q \tag{18}$$

It can be concluded that the calculation of P_m only requires I_Q which is easy to detect in the current source area.

C. MPF for a PV String under Module-Level PSCs

PV strings experience the hot spot effect when they are exposed PSCs [39]. To avoid module-level hot spots, the output port for each of the PV modules was paralleled with the diode in the opposite direction. Module-level PSCs mean that each of the PV modules has the same properties and irradiance. PV modules under different irradiations generate different short circuit currents. When a PV system operates at I_Q, if the short circuit currents for some of the PV modules are smaller than I_Q, the bypass diode belonging to these PV modules turns on. At this point, these PV modules sent nothing to the outside and are used as a load to consume the power produced by the other PV modules.

Assuming that the PV string consists of m PV modules, and m short circuit currents, I_{sc} is required in the MPF. To obtain m $I_{sc,}$ m detecting points located in the current source area of each module need to be determined. First, the detecting point is set as $U_{det(1)}$=1V, and the others are set as Equation (19):

$$U_{det(k+1)} = \sum_{n=1}^{k} U_{ocn} \tag{19}$$

Where, $U_{det(k+1)}$ is the voltage of the k+1th detecting point, and U_{ocn} is open circuit voltage of the nth PV module.

To further ensure the sampling points in the current-source area, another point was sampled in $U_{det(k+1)}$+1 V and a comparison of their currents was carried out as follows:

$$\frac{|I_1 - I_2|}{I_1} < 0.01 \tag{20}$$

Where I_1 is the current at $U_{det(k+1)}$ and I_2 is the current at $U_{det(k+1)}$ +1 V. It is assumed that these two points are in the current-source area. If this is not true, the MPF detects $U_{det(k+1)}$ +2 and $U_{det(k+1)}$ +3 to find the value of I_{sc} that is satisfied with Equation (20).

The open circuit voltage corresponding to the short circuit current can be calculated according to Equation (12). The MPPT control system takes voltage as the next detection point (the red points shown in Fig. 4). This can effectively guarantee every detecting point located within the current source area of each module. m I_{sc} in descending order is:

$I_{sc1}, I_{sc2} \ldots I_{sci} \ldots I_{scn} \ldots I_{scm}$

The current of the nth peak ($n \le m$) can be expressed as:

$$I_{mn} = k_2 I_{scn} \tag{21}$$

When the PV system is operating at I_{mn}, the short circuit currents order I_{sc1}, I_{sc2} … I_{scn-1} corresponding to the operating voltages is as follows:

$U_{op1}, U_{op2} \ldots U_{opi} \ldots U_{opn-1}$

Any operating voltage U_{opi} of the PV modules in the PV string, from 1 to n-1, can be calculated according to Equation (10), and it can be expressed as follows ($1 \le i \le n$-1):

$$U_{opi} = a \ln\left(\frac{I_{sci} - I_{mn}}{I_{D0}}\right) \tag{22}$$

As shown in Fig. 4 (in this example n=3, m=5), when the PV system works at the operating point Q_1 (I_{Q1}=I_{sc3}), it is located in the current source area of the nth PV module (where the purple shaded area, n=3). When the operating point moves from Q_1 to Q_2 in the current source area, it is easy to see that operating voltages from U_{op1} to U_{opn-1} are almost constant. Therefore, the output powers (the red and green area shown in Fig. 4) of the PV modules from 1 to n-1 are almost constant. As the operating voltage increases (the operating point from Q_1 moves to Q_2), the output power (the blue shaded area) of the nth PV module increases continuously. The operating point moves into the voltage source area of the nth PV module (the orange shaded area), and the operating point moves in the direction of the black arrow as Q_3 (the small picture in the top right hand corer of Fig. 4). The current of the operating point I_Q declines rapidly and it makes the output power of the PV string decline rapidly too. However, during the moving process from Q_1 to

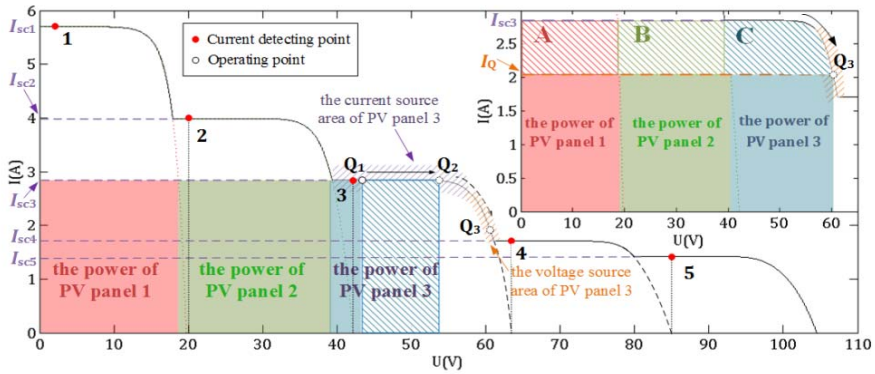

Fig. 4. Composition of power near the 3rd peak.

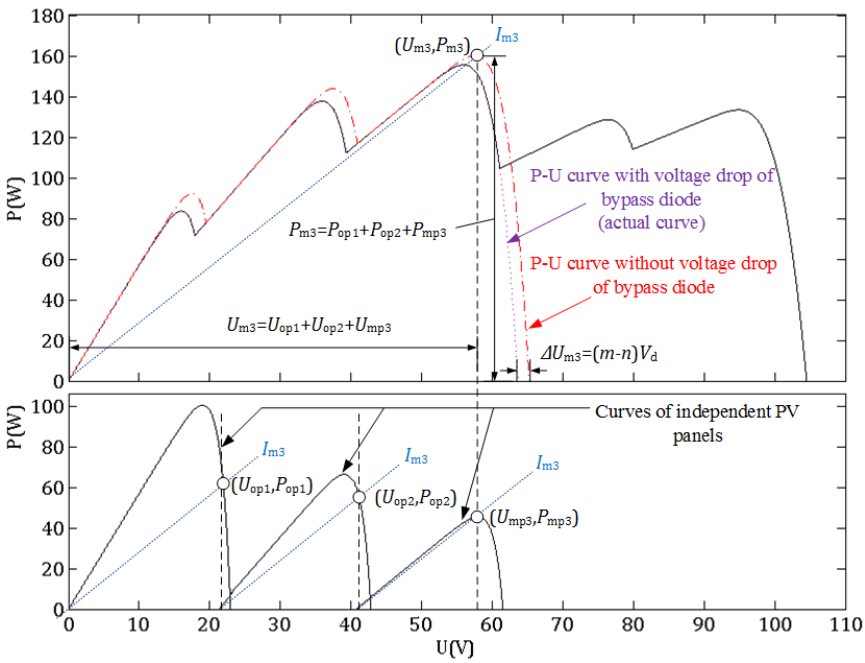

Fig. 5. Composition of voltage at MPP.

Q_2, the operating voltage of the PV modules from U_{op1} to U_{opn-1} has so little change that it can be neglected. Therefore, the position of the MPP voltage of the nth peak U_{mn} is mainly determined by the nth PV module. Equation (13) shows that the MPP voltage of the nth PV module U_{mpn} can be expressed as follows:

$$U_{mpn} = k_1 U_{ocn} \tag{23}$$

As shown in Fig. 5, the MPP voltage of the nth peak U_{mn} is composed by the operating voltage from 1 to n-1 and the MPP voltage of the nth PV module U_{mpn}. Adding them together and subtracting the voltage drop produced by the bypass diode which was turned on. The MPP voltage of the nth peak can be expressed as follows:

$$U_{mn} = \sum_{i=1}^{n-1} U_{opi} + k_1 U_{ocn} - (m-n)V_d \tag{24}$$

Consequently, the peak value P_{mn} can be given in:

$$P_{mn} = U_{mn} I_{mn} \tag{25}$$

The algorithm forecasts power values for all of the peaks and determines the maximum forecast peak. Finally, the algorithm searches the real peak value by the IP&O in the neighborhood of the forecasted value.

D. MPF for Cell-Level PSCs

In real commercial PV modules, there are cell-unit structures. They may suffer from cell-level shading conditions, which means that the same module has different levels of illumination (extreme conditions where some faulty cell's illumination is zero are not considered in this paper). A PV module was consisted of N_s (in this paper N_s=36) PV cells in series as shown in Fig. 6. A hotspot takes places when one or more of the PV cells within a PV module are shaded [40].

Under this condition, the unshaded cells of the module generate a higher short circuit current. However, the short circuit current of the whole PV module (I_{sc}(mod)) is

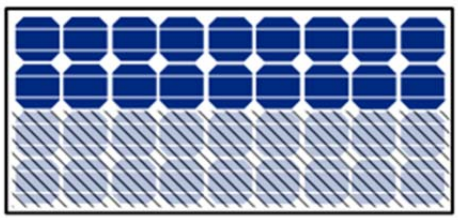

Fig. 6. Sketch map of cell-level PSCs.

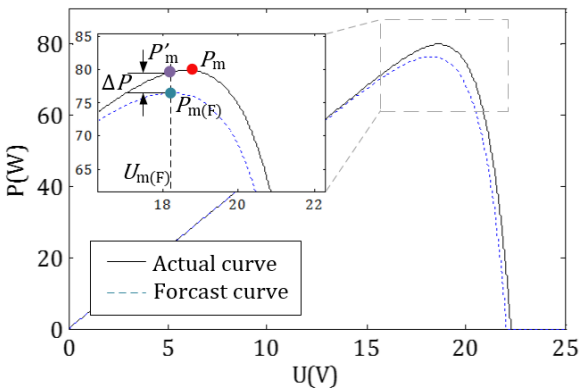

Fig. 7. Sketch map of correction module.

approximately equal to the minimum short circuit current among all of the cells.

$$I_{sc(mod)} \approx \min\left\{I_{sc1(cell)}, I_{sc2(cell)} \ldots I_{scn(cell)}\right\} \tag{26}$$

As a result, the shaded cells are forced into reverse bias and operate as a resistance to dissipate power. The hotspot deforms the *P-U* curve of the PV module, as shown in Fig. 7. After the forecast, U_m(F) and P_m(F) can be obtained. However, there is an error between P_m(F) and the real P_m. To reduce the error, the algorithm uses a correction module to detect the real power value at U_m(F), expressed as P'_m whose value is close to P_m.

To describe the degree of error cause by the cell-level PSCs, a judgment is set as follows:

$$\frac{\left|P'_m - P_{m(F)}\right|}{P_{m(F)}} \geq \varepsilon \tag{27}$$

Where ε is set as 0.01 because the errors of the MPF method under module-level PSCs are lower than 0.01.

If Equation (27) is satisfied, cell-level PSCs are thought to have occurred and the final forecasting power value is replaced by P'_m. The process of correction is illustrated in Fig. 7.

E. Heuristic Techniques: IP&O

In last part of the proposed algorithm, the IP&O is used to remedy the error of the forecasting part. As shown in Fig. 8, forecasting the MPP position is used as the initial point of the IP&O, and initial step length is *l*. When the condition $P_{i+1}<P_i$ is satisfied, the IP&O searches in the opposite direction with

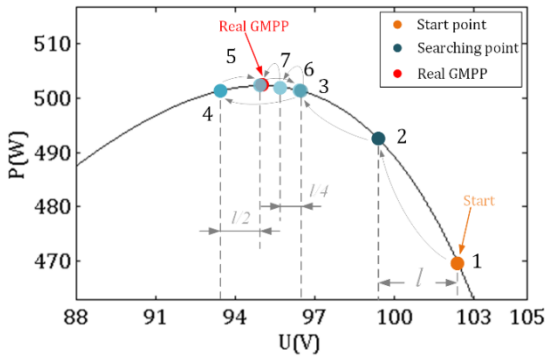

Fig. 8. Sketch map of IP&O.

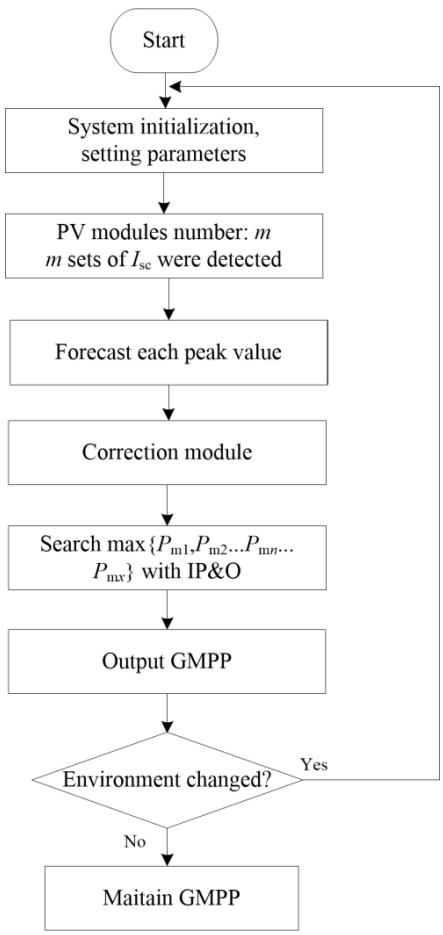

Fig. 9. Flow chart of MPF-IP&O algorithm.

l/2; when $P_{i+1}<P_i$ is satisfied again, the search direction is changed again it searches with *l*/4, and so on. When the accuracy is reached, the MPP is thought to be searched. Obviously, the IP&O is exponentially improved, which is an excellent solution to the contradiction between the speed and accuracy of the tracking.

When the external environment changes, the output characteristics of the photovoltaic array change and the maximum power point also changes. Therefore, the MPF-IP&O algorithm is restarted when the following condition is met:

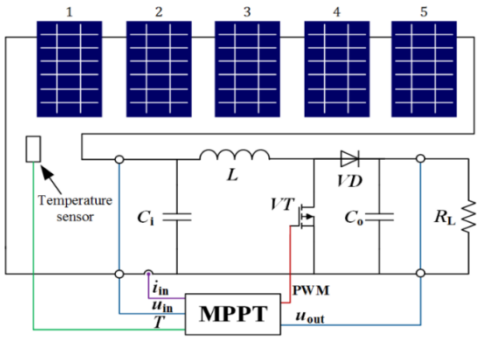

Fig. 10. Structure of PV system with Boost DC-DC converter.

TABLE I

SPECIFICATION OF PV SYSTEM

Open circuit voltage U_{oc}	22.92V
Short circuit current I_{sc}	5.70A
Peak voltage U_m	18.96V
Peak current I_m	5.30A
Capacitance (input) C_i	100μF
Capacitance (output) C_o	100μF
Inductance L	500μH
Load resistance R_L	200Ω
Switching frequency f	50kHz

$$\left|\frac{P'-P}{P}\right| \geq \Delta P \tag{28}$$

Where, P is the sampled power value after the termination of the iteration, P' is the sampled power value in the next sampling period, and ΔP is the power change tolerance. The MPF-IP&O algorithm flow chart is shown in Fig. 9.

IV. SIMULATION RESULTS AND ANALYSIS

The heuristic technique P&O and the intelligent algorithm PSO are widely used in MPPT algorithms, and they are considered as standard benchmarks for any new MPPT. To verify the performance of the proposed algorithm, a test simulation is designed, in which the proposed algorithm is compared with the P&O and PSO. As shown in Fig. 10, the MPPT system is composed of three parts: a PV string, a Boost converter and MPPT modules. The PV string consists of five PV modules (m=5), and each of the modules has 36 cells in series. The specifications of the PV system are shown in TABLE I. In the P&O, the perturbation step ΔU=2V. In the PSO, the population number N_p=5, the inertia weight ω=0.4, the acceleration constants c_1=0.8 and c_2=1.0. In the MPF-IP&O, the step length l=0.5V.

A. Uniform Irradiation Condition (UIC)

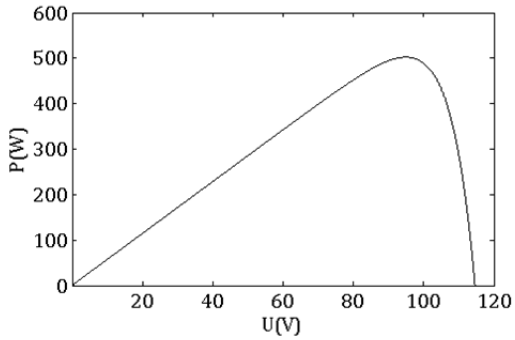

Fig. 11. *P-U* curve of PV string under UIC.

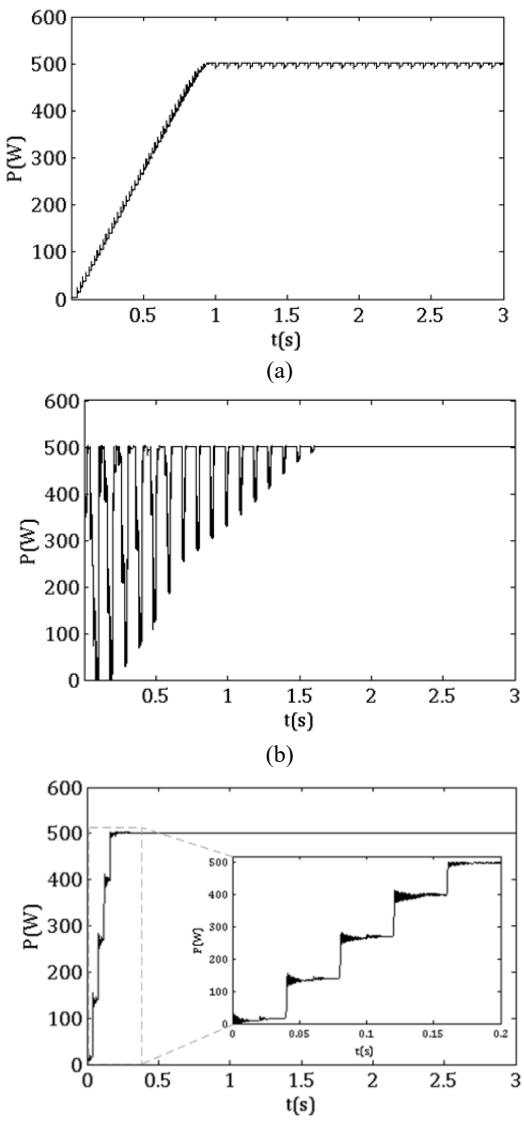

Fig. 12. Tracking trajectories under UIC. (a) P&O, (b) PSO, (c) MPF-IP&O.

Fig. 11 shows the *P-U* characteristic of the PV string under the UIC. In this condition, S=1000W/m^2, T=25℃, and the GMPP value is 502.3W. The tracking trajectories of the P&O, PSO, and MPF-IP&O are presented in Fig. 12.

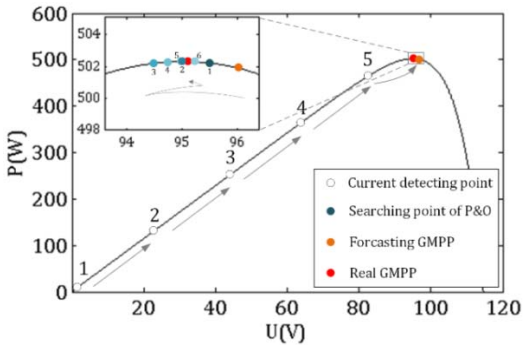

Fig. 13. Sketch map of MPF-IP&O under UIC.

TABLE II

FORECASTED PEAK VALUES OF MPF UNDER UIC. (F=FORECASTED, R=REAL)

n	I_{scn}/A	$U_{mn(F)}$/V	$P_{mn(F)}$/W	$P_{mn(R)}$/W	Error e
1	5.70	\	\	\	\
2	5.70	\	\	\	\
3	5.70	\	\	\	\
4	5.70	\	\	\	\
5*	5.70	95.12	504.12*	502.30	0.382%

It can be seen from Fig. 12 that the P&O takes about 0.94s, the PSO take about 1.60s, and the MPF-IP&O takes about 0.26s to reach the MPP. Compared with the P&O and PSO, the proposed algorithm saves 72.34% and 83.75% in terms of tracking time, respectively. The tracking efficiency (the ratio of the tracked MPP and the real GMPP value) of the P&O, the PSO and the proposed algorithm are 98.85%, 99.99%, and 99.99%, respectively. The tracking data of the proposed algorithm under UIC is shown in TABLE II. It is easy to see that the forecasted peak values are close to the real value.

As shown in Fig. 13, the range that has been searched by the IP&O is just 1.36% of the total. It is easy to see that the proposed algorithm has a better time response and a higher accuracy in comparison with the P&O and PSO. The MPF reduces the searching range tremendously and shortens the tracking time. The local search of the IP&O greatly enhances THE searching accuracy. The combination of the MPF and the IP&O fully utilizes characteristics and advantages of them both.

B. Module-Level Partial Shading Condition (PSC)

This investigation is implemented to assess and compare the performances of the P&O, the PSO, and the proposed algorithm under module-level PSCs. In this condition, the irradiance levels S of five PV modules are set to 1000, 750, 650, 500 and 200 W/m^2, and T=-10℃. Fig. 14 shows the *P-U* curve of the PV string under PSCs. It is easy to see that there are five peaks in the curve and that the 4th peak is the GMPP whose value is 215.6W. The tracking trajectories of the P&O, PSO, and MPF-IP&O are shown in Fig. 15.

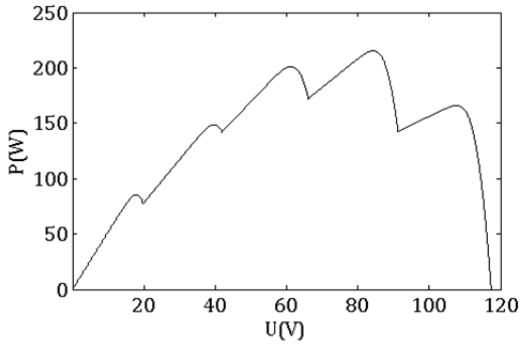

Fig. 14. *P-U* curve of PV string under module-level PSC.

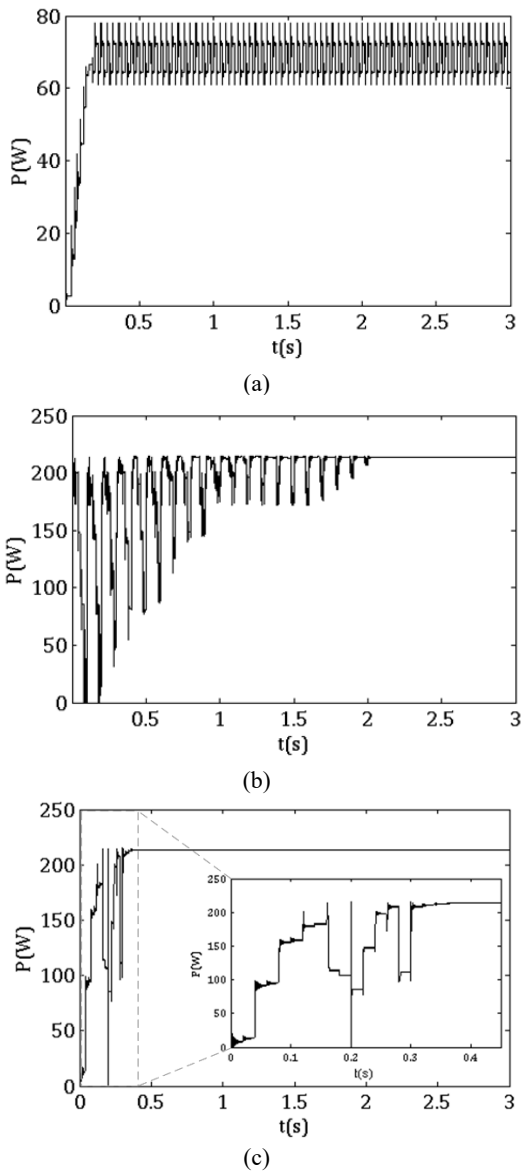

Fig. 15. Tracking trajectories under PSC. (a) P&O, (b) PSO, (c) MPF-IP&O.

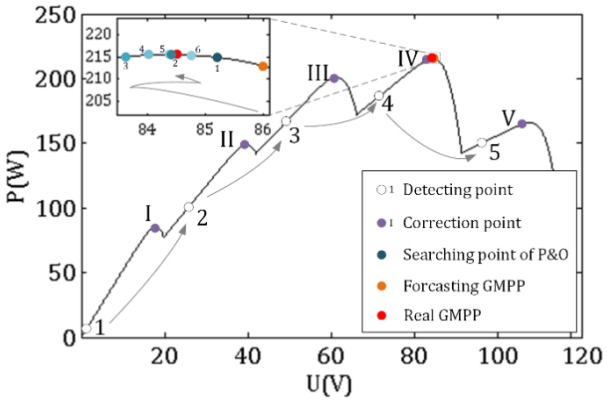

Fig. 16. Sketch map of MPF-IP&O under PSC.

TABLE III

FORECASTED PEAK VALUES OF MPF UNDER PSC. (F=FORECASTED, R=REAL)

n	I_{scn}/A	$U_{mn(F)}$/V	$P_{mn(F)}$/W	$P_{mn(R)}$/W	Error e
1	5.200	17.74	85.63	85.54	0.106%
2	3.900	41.45	149.14	148.80	0.226%
3	3.380	64.60	201.43	201.10	0.165%
4*	2.680	85.89	213.74*	215.60	0.862%
5	1.610	109.85	164.78	165.90	0.678%

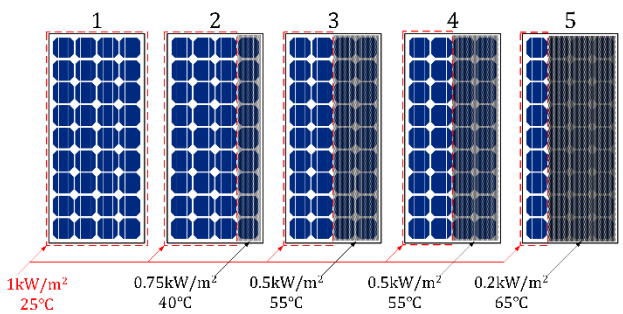

Fig. 17. PV string under Cell-level PSC.

As shown in Fig. 15, the P&O gets trapped in a LMPP but the PSO and MPF-IP&O find the GMPP. To reach the GMPP, it takes the PSO 2.02s and the MPF-IP&O only 0.38s. The proposed algorithm saves 81.19% of the tracking time compared with the PSO. The tracking efficiency of the P&O, the PSO and the proposed algorithm are 31.83%, 99.27%, and 99.98%, respectively. The tracking data of the proposed algorithm under PSCs is shown in TABLE III. It is easy to see that the forecasted peak values are close to the real values. As shown in Fig. 16, compared with the P&O and the PSO, the proposed algorithm has the MPF capable of preventing algorithm from getting trapped in a LMPP, a simple structure, and it overcomes blindness and randomness in searching.

As shown in Fig. 16, the range searched with the IP&O is just 1.66% of the total. The MPF reduces the searching range

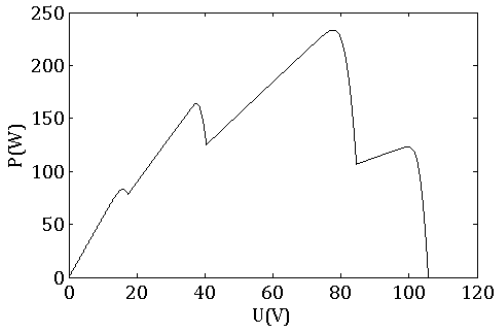

Fig. 18. *P-U* curve of PV string under cell-level PSC.

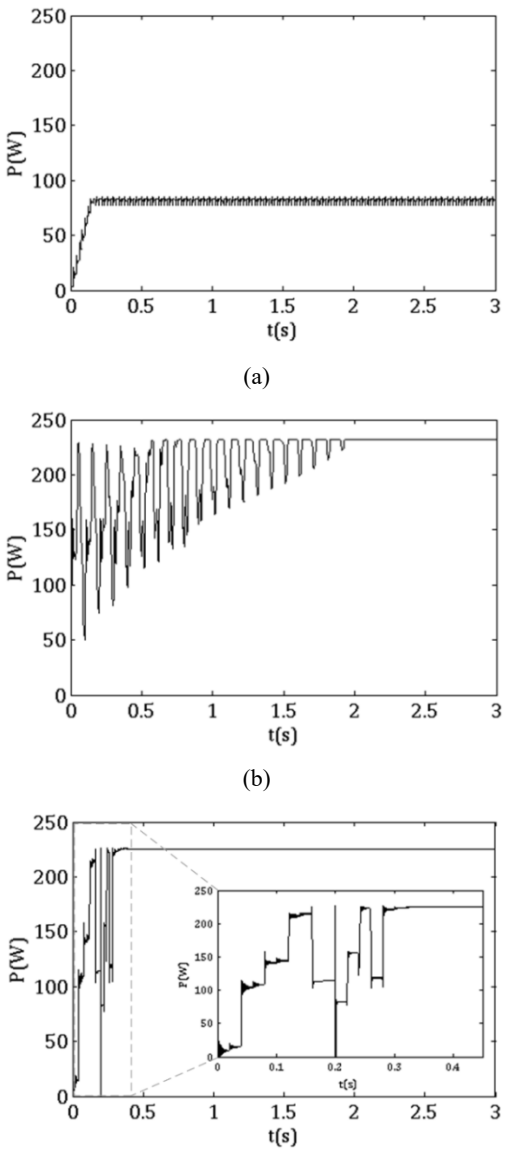

Fig. 19. Tracking trajectories under cell-level PSC. (a) P&O, (b) PSO, (c) MPF-IP&O.

tremendously and shortens the tracking time, while the local search of the IP&O greatly enhances the searching accuracy. The combination of the MPF and the IP&O fully utilizes the

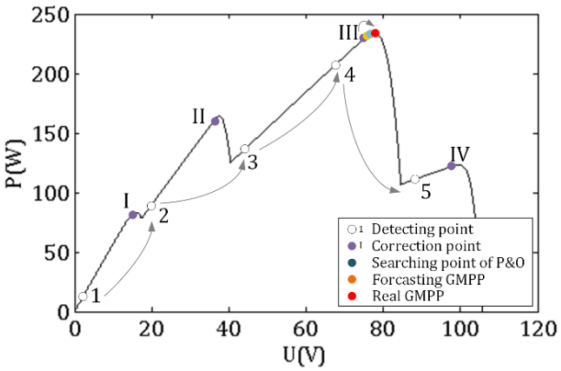

Fig. 20. Sketch map of MPF-IP&O under cell-level PSC.

characteristics and advantages of them both. Hence, proposed algorithm has a better time response and a higher accuracy in comparison with the P&O and PSO.

C. Cell-level Partial Shading Condition (PSC)

Fig. 17 shows the environmental conditions of the PV string under cell-level PSCs, and Fig. 18 shows the P-U curve. It is easy to see that there are four peaks in the curve and that the 3rd peak is the GMPP whose value is 233.40W. The tracking trajectories of the P&O, PSO, and MPF-IP&O are shown in Fig. 19.

As shown in Fig. 19, the P&O gets trapped in a LMPP but the PSO and MPF-IP&O find the GMPP. To reach the GMPP, it takes the PSO 1.96s and it takes the proposed algorithm only 0.38s. The proposed algorithm saves 80.21% in terms of the tracking time compared with the PSO. The tracking efficiency of the P&O, the PSO and the proposed algorithm are about 35.65%, 99.39%, and 99.97%, respectively. The tracking data of the proposed algorithm under cell-level PSCs is shown in TABLE IV. It is easy to see that the forecasted peak values without correction have an error when compared to the real value. After correction, the forecasted peak values are close to the real values. The correction module ensures that the MFA still works well under cell-level PSCs. As shown in Fig. 19, compared with the P&O and PSO, the proposed algorithm has the MPF capable of preventing the algorithm getting trapped in a LMPP, a simple structure, and it overcomes blindness and randomness in searching.

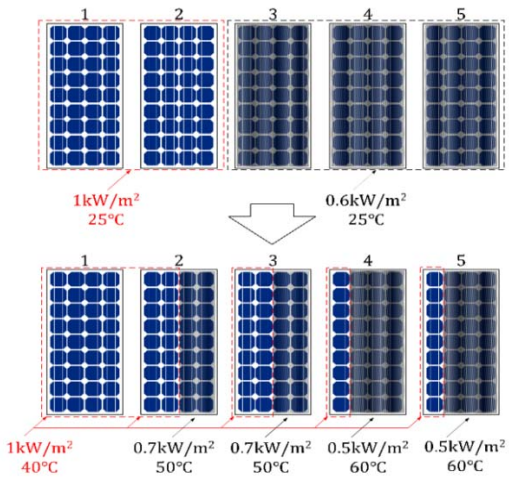

Fig. 21. PV string under Environment Suddenly Change Condition.

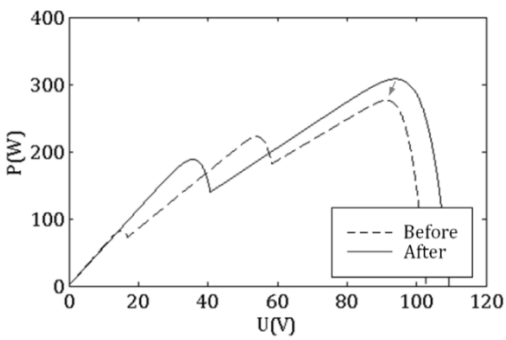

Fig. 22. *P-U* curve of PV string under cell-level PSC.

As shown in Fig. 20, the range searched with the IP&O is just 2.43% of the total. The MPF narrows the searching range tremendously, and the local search of the IP&O greatly enhances the searching accuracy. The combination of the MPF and the IP&O fully utilizes the characteristics and advantages of them both. Hence, the proposed algorithm has a better time response and a higher accuracy in comparison with the P&O and PSO.

D. Environment Suddenly Change Condition

In order to investigate and verify the performance and accuracy of the proposed algorithm under the environment

TABLE IV

FORECASTED PEAK VALUES OF MPF UNDER CELL-LEVEL PSC. (F=FORECASTED, R=REAL)

n	I_{scn}/A	$U_{mn(F)}$/V	$P_{mn(F)}$/W	$P_{mn(R)}$/W	Error e	P'_{mn}/W (Corrected)	Error e' (Corrected)
1	5.700	15.75	83.46	83.25	0.270%	\	\
2	4.472	37.27	154.98	164.10	5.561%	163.90	0.122%
3	3.079	\	\	\	\	\	\
4*	3.078	76.09	216.59*	233.40	7.202%	231.50	0.814%
5	1.250	98.12	114.04	123.10	7.361%	122.10	0.812%

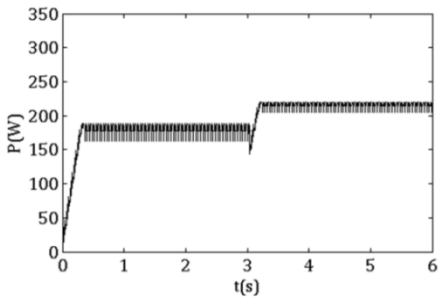

(a)

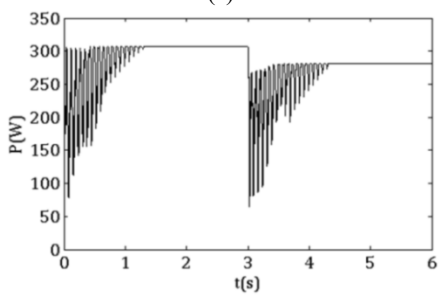

(b)

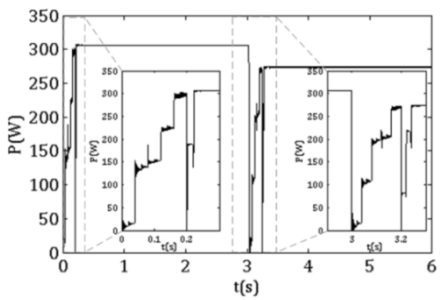

(c)

Fig. 23. Tracking trajectories under environment suddenly change condition. (a) P&O, (b) PSO, (c) MPF-IP&O.

Fig. 24. PV string under cell-level PSC.

suddenly change condition, a step change is applied to the solar irradiance and temperature at the 3rd second. The *P-U* curve change is shown in Fig. 22. In the interval 0-3s, there are two peaks in the *P-U* curve and the global MPP is 308.10 W. In the interval 3-6s, there are three peaks in the *P-U* curve and the global MPP is 276.30 W. The trajectories of the P&O, PSO, and MPF-IP&O are plotted in Fig. 23. This figure shows that the PSO and MPF-IP&O can find the global MPP when the environment suddenly changes while the P&O converges to a local MPP.

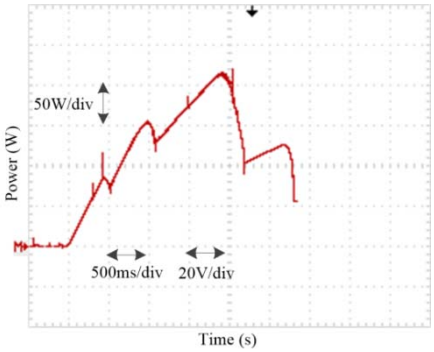

(a)

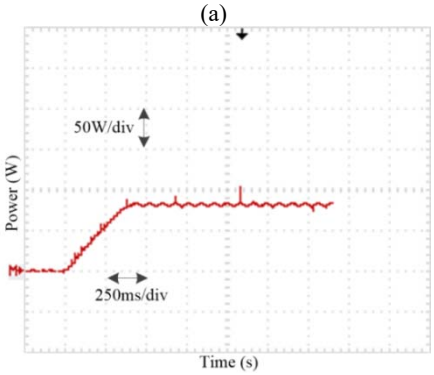

(b)

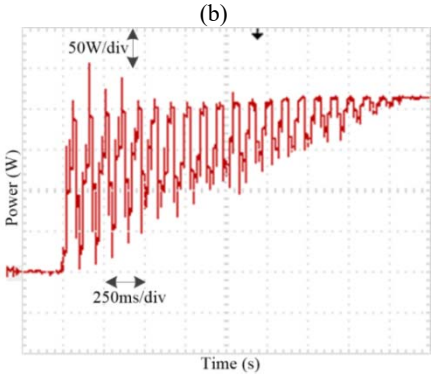

(c)

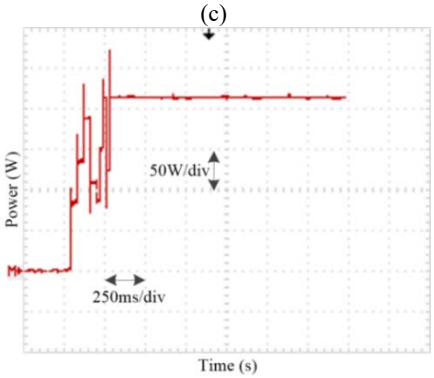

(d)

Fig. 25. Experimental waveforms: (a) *P-U* curve of PV string under PSC, and tracking trajectories of (b) PAO; (c) PSO; (d) MPF-IP&O.

V. Experiment Results and Analysis

To verify the effectiveness of the proposed algorithm, a five series PV configuration is exposed to four different shadings. The specifications of the experimental system are

same as the simulated one which is shown in TABLE I. In this experiment a DSP (TI TMS320F28335) is used to control the DC/DC boost converter. To produce four different shadings, five PV modules were shaded with different translucent membrane as shown in Fig. 24. In the P&O, ΔU=1V; in the PSO, the population number N_p=5, ω=0.4, c_1=0.8 and c_2=1.0; in the MPF-IP&O, the step length l=0.5V.

The *P-U* curve shown in Fig. 25 (a) was obtained by utilizing global scanning method. The scan step was set as 0.8V and the sampling time was set as 20 ms. It is easy to see that there are four peaks in the *P-U* curve and that the global peak value is about 216.5W. The tracking trajectories of the three methods are shown in Fig. 25. It is easy to see that the P&O gets trapped in a local MPP whose value is about 83.5W. To track the GMPP, it takes the PSO and the proposed algorithm about 2.12s and 0.38s, respectively. It is easy to see that the proposed algorithm can exact the GMPP and shortens tracking time sharply. The tracking efficiency of the PSO and the MFP-IP&O are 99.56% and 99.97%, respectively. Hence, the proposed algorithm has a better time response and a higher accuracy when compared with the P&O and PSO.

VI. Conclusion

In this paper, a hybrid MPPT technique with global search capability for PV strings is proposed. A novel MPF, without additional irradiance sensors or complex computations, is devised to effectively reduce the blindness of global searches under unknown environments, which saves a lot of search time. An IP&O is used to remedy the error of the forecasting part. Its performance is compared with the P&O and PSO. Simulation and experimental results show that the proposed algorithm outperforms both of them in terms of tracking speed and accuracy under PSCs.

Appendix

Nomenclature

a	ideality factor parameter defined as $a \equiv n_1 kT/q$	I_{D0}	saturation current of photovoltaic cells in the absence of light (A)
a_{ref}	ideality factor parameter at stand reference conditions (SRC)	$I_{D0,ref}$	saturation current at SRC (A)
A	PN junction area	I_{VD}	diode current (A)
k	Boltzmann's constant (1.38066×10^{-23} J/K)	I_{sc}	short circuit current (A)
n_1	usual ideality factor	$I_{sc,ref}$	short circuit current at SRC (A)
q	electron charge (1.60218×10^{-19} C)	I_{scn}	short circuits of nth PV module (A)
R_L	load resistance (Ω)	I_L	load current (A)
R_s	series resistance (Ω)	I_Q	current at operating point Q (A)
N_C, N_V	the effective density of states in the conduction band and valence band	I_m	current at MPP (A)
N_A, N_D	The concentration of acceptor and donor impurity	$I_{m,ref}$	current at MPP and SRC (A)
D_n, D_p	diffusion coefficient of electrons and holes	I_{mn}	current of nth PV module at MPP (A)
τ_n, τ_p	Minority carrier lifetime of electrons and holes	I'_{mn}	forecasting current of nth PV module at MPP (A)
E_g	bandgap of semiconductor material (J)	U_{oc}	open circuit voltage (V)
$E_{g,ref}$	energy bandgap at reference temperature (1.121 eV for silicon) (J)	$U_{oc,ref}$	open circuit voltage at SRC (V)
S	total absorbed irradiance (W/m^2)	U_{ocn}	open circuit voltage of nth PV module (V)
T	cell temperature (℃)	U_Q	voltage at operating point Q (V)
T_{ref}	cell temperature at SRC (℃)	U_m	voltage at MPP (V)
k_1	voltage factor	$U_{m,ref}$	voltage at MPP and SRC (V)
k_2	current factor	U_{mn}	voltage of nth peak (V)
P_Q	power at operating point Q (W)	U'_{mn}	forecasting voltage of nth peak (V)
P_m	power at MPP (W)	U_{mpn}	voltage of nth PV module at MPP (V)
P_{mn}	power of nth peak (W)	U_{opi}	operating voltage of ith PV module (V)
P_{opi}	operating power of ith PV module (W)	U_L	load voltage (V)
P_{mpn}	power of nth PV module at MPP (W)		

REFERENCES

[1] N. Fernia, G. Petrone, G. Spagnuolo, and M. Vitelli, "Optimization of perturb and observe maximum power point tracking method," *IEEE Trans. Power Electron*., Vol. 20, No. 4, pp. 963-973, Jul. 2005.

[2] L. Piegari and R. Rizzo, "Adaptive perturb and observe algorithm for photovoltaic maximum power point tracking," *IET Renewable Power Generation*, Vol. 4, No. 4, pp. 317-328, Jul. 2010.

[3] N. Fermia, D. Granozio, G. Petrone, and M. Vitelli, "Predictive & adaptive MPPT perturb and observe method," *IEEE Trans. Aerosp. Electron. Syst*., Vol. 43, No. 3, pp. 935-950, Jul. 2007.

[4] A. K. Abdelsalam, A. M. Massoud, S. Ahmed, and P. N. Enjeti, "High-performance adaptive perturb and observe MPPT technique for photovoltaic-based microgrids," *IEEE Trans. Power Electron.,* Vol. 26, No. 4, pp. 1010-1021, Apr. 2011.

[5] J. Li and H. Wang, "A novel stand-alone PV generation system based on variable step size INC MPPT and SVPWM control," in *IEEE 6th International Power Electronics and Motion Control Conference(IPEMC)*, pp. 2155-2160, Jul. 2009.

[6] F. Liu, S. Duan, F. Liu, B. Liu, and Y. Kang, "A variable step size INC MPPT method for PV systems," *IEEE Trans. Ind. Electron.*, Vol. 55, No. 7, pp. 2622-2628, Jul. 2008.

[7] A. Safari and S. Mekhilef, "Simulation and hardware implementation of incremental conductance MPPT with direct control method using Cuk converter," *IEEE Trans. Ind. Electron.*, Vol. 58, No. 4, pp. 1154-1161, Apr. 2011.

[8] Q. Fu and N. Tong, "A new fuzzy control method based on PSO for maximum power point tracking of photovoltaic system," in *2011 International Conference on Computer Science and Network Technology (ICCSNT),* Vol. 3, pp. 1487-1491, Apr. 2012.

[9] B. N. Alajmi, K. H. Ahmed, S. J. Finney, and B. W. Williams, "Fuzzy-logic-control approach of a modified hill-climbing method for maximum power point in microgrid standalone photovoltaic system," *IEEE Trans. Power Electron*., Vol. 26, No. 4, pp.1022–1030, Apr. 2011.

[10] W. Xiao and W. G. Dunford, "A modified adaptive hill climbing MPPT method for photovoltaic power systems," in *IEEE 35th Annual Power Electronics Specialists Conference (PESC)*, pp.1957-1963, Jun. 2004.

[11] X. Li, H. Wen, L. Jiang, Y. Hu, and C. Zhao, "An improved beta method with auto-scaling factor for photovoltaic system," *IEEE Trans. Ind. Appl.*, Vol. 52, No.5, pp. 4281-4291, Sep./Oct. 2016.

[12] X. Li, H. Wen, L. Jiang, E. G. Lim, Y. Du, and C. Zhao, "Photovoltaic modified β-parameter-based MPPT method with fast tracking," *Journal of Power Electronics*, Vol. 16, No. 1, pp. 9-17, Jan. 2016.

[13] Y. Hu, W. Cao, J. Ma, S. J. Finney, and D. Li, "Identifying PV module mismatch faults by a thermography-based temperature distribution analysis," *IEEE Trans. Device Mater. Rel.*, Vol. 14, No. 4, pp. 951-960, Dec. 2014.

[14] Y. Hu, J. Zhang, W. Cao, J. Wu, G. Y. Tian, S. J. Finney, and J. L. Kirtley, "Online two-section PV array fault diagnosis with optimized voltage sensor locations," *IEEE Trans. Ind. Electron.*, Vol. 62, No. 11, pp. 7237-7246, Nov. 2015.

[15] H. Patel and V. Agarwal, "Maximum power tracking scheme for PV systems operating under partially shaded conditions," *IEEE Trans. Ind. Electron.*, Vol. 55, No. 4, pp. 1689-1698, Apr. 2008.

[16] R. Bruendlinger, B. Bletterie, M. Milde, and H. Oldenkamp, "Maximum power point tracking performance under partially shaded PV array conditions," in *Proceedings of 21st EUPVSEC*, pp. 2157-2160, Jan. 2006.

[17] J. Y. Shi, W. Zhang, Y. G. Zhang, F. Xue, and T. Yang, "MPPT for PV systems based on a dormant PSO algorithm," *Electric Power Systems Research*, Vol. 123, pp. 100-107, Jun. 2015.

[18] Y.-H. L, S.-C. Huang, J.-W. Huang, and W.-C. Liang, "A particle swarm optimization-based maximum power point tracking algorithm for PV systems operating under partially shaded conditions," *IEEE Trans. Energy Convers.* Vol. 27, No. 4, pp. 1027-1035, Dec. 2012.

[19] L. L. Jiang, D. L. Maskell, and J. C. Patra, "A novel ant colony optimization-based maximum power point tracking for PV systems under partially shaded conditions," *Energy and Buildings*, Vol. 58, pp. 227-236, Mar. 2013.

[20] K. Sundareswaran, S. Peddapati, and S. Palani, "MPPT of PV systems under partial shaded conditions through a colony of flashing fireflies," *IEEE Trans. Energy Convers.,* Vol. 29, No. 2, pp. 463-472, Jun. 2014.

[21] Y. M. Safarudin, A. Priyadi, M. H. Purnomo, and M. Pujiantara, "Maximum power point tracking algorithm for photovoltaic system under partial shaded condition by means updating β firefly technique," in *6th International Conference on Information Technology and Electrical Engineering (ICITEE),* pp. 1-5, Oct. 2014.

[22] J. Y. Shi, F. Xue, Z. J. Qin, W. Zhang, L. T. Ling, and T. Yang, "Improved global maximum power point tracking for photovoltaic system via cuckoo search under partial shading conditions," *Journal of Power Electronics*, Vol. 16, No. 1, pp. 287-296, Jan. 2016.

[23] J. Ahmed and Z. Salam, "A critical evaluation on maximum power point tracking methods for partial shading in PV systems," *Renewable and Sustainable Energy Reviews*, Vol. 47, pp. 933-953, Jul. 2015.

[24] K. Sundareswaran, P. Sankar, P. S. R. Nayak, S. P. Simon, and S. Palani, "Enhanced energy output from a PV system under partial shaded conditions through artificial bee colony," *IEEE Trans. Sustain. Energy*, Vol. 6, No. 1, pp. 198-209, Jan. 2015.

[25] L. Zhang, A. Al-Amoudi, and Y. Bai, "Real-time maximum power point tracking for grid-connected PV systems," in *8th International Conference on Power Electron*. *Variable Speed Drives (IEE Conf. Publ. No.475),* pp. 124-129, Sep. 2000.

[26] X. Wang, H. Z. Jiang, L. Yang, and P. Yan, "A new method of MPPT control based on the model of PV array," in *Asia-Pacific Power Energy Engineering Conference (APPEEC)*, pp. 11-18, Apr. 2011.

[27] L. V. Hartmann, M. A. Vitorino, M. B. R. Correa, and A. M. N. Lima, "Combining model-based and heuristic techniques for fast tracking the maximum power point of PV systems," *IEEE Trans. Power Electron.*, Vol. 28, No. 6, pp. 2875-2885, Jun. 2013.

[28] L. Cristaldi, M. Faifer, M. Rossi, and S. Toscani, "An improved model-based maximum power point tracker for PV modules," *IEEE Trans. Instrum. Meas.*, Vol. 63, No. 1, pp. 63-71, Jan. 2014.

[29] Y. Mahmoud, M. Abdelwahed, and E. F. El-Saadany, "An enhanced MPPT method combining model-based and heuristic techniques," *IEEE Trans. Sustain. Energy*, Vol. 7, No. 2, pp. 576-585, Apr. 2016.

[30] Y. Mahmoud and E. F. El-Saadany, "Fast power-peaks

estimator for partially shaded PV system," *IEEE Trans. Energy Convers.*, Vol. 31, No. 1, pp. 206-217, Mar. 2016.
[31] Y. Hu, W. Cao, J. Wu, B. Ji, and D. Holliday, "Thermography-based virtual MPPT scheme for improving PV energy efficiency under partial shading conditions, *IEEE Trans. Power Electron.*, Vol. 29, No. 11, pp. 5667-5672, Nov. 2014.
[32] M. C. Alonso-Garcia, J. M. Ruiz, and F. Chenlo, "Experimental study of mismatch and shading effects in the I-V characteristic of PV module," *Solar Energy Materials and Solar Cells,* Vol. 90, No. 3, pp. 329-340, Feb. 2006.
[33] S. S. Li and X. Zhang, "Improved method to build mathematic engineering model of PV module," *Electric Power Automation Equipment*, Vol. 35, pp. 108-112, Sep. 2015.
[34] Y. Mahmoud, W. Xiao, and H. H. Zeineldin, "A simple approach to modeling and simulation of PV modules," *IEEE Trans. Sustain. Energy*, Vol. 3, No. 1, pp. 185-186, Jan. 2012.
[35] S. Liu and R. A. Dougal, "Dynamic multi-physics model for solar array," *IEEE Trans. Energy Convers*, Vol. 17, No. 2, pp. 285-294, Jun. 2002.
[36] W. De Soto, S. A. Klein, and W. A. Beckman, "Improvement and validation of a model for photovoltaic array performance," *Solar Energy*, Vol. 80, No. 1, pp. 78-88, Jan. 2006.
[37] L. Zhou, Y. Chen, K. Guo, and F. C. Jia, "New approach for MPPT control of PV system with mutative-scale dual-carrier chaotic search," *IEEE Trans. Power Electron.*, Vol. 26, No. 4, pp. 1038-1048, Apr. 2011.
[38] M. A. S. Masoum, H. Dehbonei, and E. F. Fuchs, "Theoretical and experimental analyses of PV systems with voltage and current-based maximum power point tracking," *IEEE Trans. Energy Convers.*, Vol. 17, No. 4, pp. 514-522, Dec. 2002.
[39] A. Kouchaki, H. Iman-Eini, and B. Asaei, "A new maximum power point tracking strategy for PV arrays under uniform and non-uniform insolation conditions," *Solar Energy*, Vol. 91, pp. 221-232, May 2013.
[40] D. Rossi, M. Omana, D. Giffreda, and C. Metra, "Modeling and detection of hotspot in shaded photovoltaic cells," *IEEE Trans. Very Large Scale Integr. (VLSI) Syst.*, Vol. 23, No. 6, pp. 1031-1039, Jun. 2015.

Ji-Ying Shi was born in Tianjin, China, in 1959. He received his M.S. and Ph.D. degrees from Tianjin University, Tianjin, China, in 1993 and 1996, respectively. He was a Visiting Scholar and a Post-doctoral Student with The Hong Kong University of Science and Technology, Hong Kong, China, from July 1996 to November 1999. He is presently working as an Associate Professor in the Department of Electrical Engineering and Automation, Tianjin University. His current research interests include power electronic techniques, renewable energy, and soft switching techniques.

Fei Xue was born in Guyuan, China, in 1994. He received his B.S. and M.S. degrees in Electrical Engineering from Tianjin University, Tianjin, China, in 2014 and 2016, respectively. He is presently working as an Associate Engineer in the Electric Power Research Institute, State Grid Ningxia Electric Power Company (NEPC), Yinchuan, China. His current research interest includes maximum power point tracking technology, renewable energy, and the modeling and planning of distribution networks.

Le-Tao Ling was born in China, in 1993. He received his B.S. degree in Electrical Engineering from Guangzhou University, Guangzhou, China, in 2015. Since 2015, he has been working towards his M.S. degree in the School of Electrical Engineering and Automation, Tianjin University, Tianjin, China. His current research interests include the maximum power point tracking of photovoltaic and wind power systems, renewable energy and power electronic techniques.

Xiao-Fei Li was born in Jinan, China, in 1993. She received her B.S. degree in Electrical Engineering and Automation from Tianjin University, Tianjin, China, in 2015. She presently working towards her M.S. degree at the State Grid Electric Power Research Institute, Nanjing, China. Her current research interests includes carbon markets.

Zi-Jian Qin was born in Laiwu, China, in 1990. He received his B.S. degree in Electrical Engineering and Automation from Qufu Normal University, Rizhao, China, in 2014. He is presently working towards his M.S. degree at Tianjin University, Tianjin, China. His current research interests includes the modeling and simulation of microgrids and the maximum power point tracking of photovoltaic and wind energy generation systems.

Ya-Jing Li was born in Handan, China, in 1995. She received her B.S. degree in Electrical Engineering and Automation from Yanshan University, Qinhuangdao, China, in 2016. She is presently working towards her M.S. degree at Tianjin University, Tianjin, China. Her current research interests include the modeling and planning of active distribution networks, renewable energy and power electronic techniques.

Ting Yang is presently working as a Chair Professor of Theory and Advanced Technology of Electrical Engineering, in the School of Electrical Engineering and Automation, Tianjin University, Tianjin, China. He has authored or co-authored four books and over 80 publications in technical journals and conference proceedings. Professor Yang is a Member of the International Society for Industry and Applied Mathematics, a Senior Member of the Chinese Institute of Electronics, a Fellow of the Circuit and System Committee, and a Fellow of the Theory and Advanced Technology of Electrical Engineering Committee. He was a winner of an Education Ministry's New Century Excellent Talents Supporting Plan. His current research interests include power electronic techniques and renewable energy.